

# Towards Imperceptible Adversarial Image Patches Based on Network Explanations

Yaguan Qian, Jiamin Wang, Bin Wang, Zhaoquan Gu, Xiang Ling, and Chunming Wu

**Abstract**—The vulnerability of deep neural networks (DNNs) for adversarial examples has attracted more attention. Many algorithms are proposed to craft powerful adversarial examples. However, these algorithms modifying the global or local region of pixels without taking into account network explanations. Hence, the perturbations are redundancy and easily detected by human eyes. In this paper, we propose a novel method to generate local region perturbations. The main idea is to find the contributing feature regions (CFRs) of images based on network explanations for perturbations. Due to the network explanations, the perturbations added to the CFRs are more effective than other regions. In our method, a soft mask matrix is designed to represent the CFRs for finely characterizing the contributions of each pixel. Based on this soft mask, we develop a new objective function with inverse temperature to search for optimal perturbations in CFRs. Extensive experiments are conducted on CIFAR-10 and ILSVRC2012, which demonstrate the effectiveness, including attack success rate, imperceptibility, and transferability.

**Index Terms**—Adversarial examples, Contributing feature regions, Adversarial patches.

## I. INTRODUCTION

THE development of deep learning technology has promoted the successful application of deep neural networks (DNNs) in various fields, such as image classification [1], [2], computer vision [3], [4], natural language processing [5], [6], etc. In particular, convolutional neural networks (CNNs), a typical DNN, have shown excellent performance applied in image classification. However, many works have shown that CNNs are extremely vulnerable to *adversarial examples* [7]. An adversarial example is crafted from a clean example added by well-designed perturbations that are almost imperceptible to human eyes but can easily fool classifiers. Besides, adversarial examples provide a valuable and beneficial perspective for understanding the behaviors of CNNs [8].

Researchers have proposed a variety of methods to craft adversarial examples, such as L-BFGS [7], FGSM [8], I-FGSM [9], PGD [10], and C&W [11]. Goodfellow et al. [8] argued that the primary cause of the adversarial instability is the linear nature and the high dimensionality. Later work

[12] studied the linearity hypothesis further and argued that adversarial examples exist when the classification boundaries lie close to the manifold of sampled data. D. Su et al. [13] empirically found out the trade-off of accuracy and robustness and revealed that the robustness may be the cost of accuracy. All the aforementioned works either generate specific adversarial examples by some optimization techniques or attempt to leverage adversarial phenomena to understand CNN's behavior to minor perturbations in visual inputs. On the contrary, we attempt to utilize the explanation of CNNs to generate more effective adversarial examples.

We are inspired by the work of CAM [14] and Grad-CAM [15], which are considered as one of the state-of-the-art visual explanations to CNNs. As shown in Fig. 1, only a small region of an object contributes the most to the classification, which is similar to human attention mechanisms. This special region is referred to as a *contributing feature* (CFR) in this paper. With this observation, we speculate that adding perturbations to the CFR will be more effective than previous methods. We further design a soft mask matrix to represent the CFRs for finely characterizing the contributions of each pixel. Based on this soft mask, we develop a new objective function to search for optimal perturbations in CFRs. The objective function we optimize is consist of two parts: the amplitude of the perturbations and the loss of the generated adversarial examples. To avoid the perturbation variable stopping update when the objective function goes to zero, we also introduce a hyperparameter  $T$  named *inverse temperature* inspired by the distillation idea in [16].

Since the CFRs represent the attention regions of an object, our method crafting adversarial perturbations on CFRs is considered at a semantic level, while previous works mostly focus on perturbations at a pixel level. The typical methods like FGSM [8] and C&W [11] perturb all the pixels in an image without considering their semantics. Although some methods perturb local image regions like JSMA [17] and one-pixel attacks [18], they do not take account of the interaction between the neighboring pixels with perturbations, i.e., the perturbed pixels may do not form a continuous region. Similar to our work, some local continuous region attacks are proposed, which are named as patch attacks [19], [20] or sticker attacks [21]. Hence, our perturbations on CFR can be considered as some forms of patch attacks. However, our method is different from existing patch attacks in three aspects. The first is that the shape of patches or stickers is regular, while our CFR's shape is arbitrary. The second is that the location of patches or stickers is optionally determined by the adversary, while our CFR is located by Grad-CAM at a semantic level. Finally,

Y. Qian, J. Wang are with the School of Big-Data Science, Zhejiang University of Science and Technology, Hangzhou 310023, China. (e-mail: qianyaguan@zust.edu.cn, 1621099083@qq.com)

B. Wang is with the Network and Information Security Laboratory of Hangzhou Hikvision Digital Technology Co., Ltd. Hang Zhou 310052, China. (e-mail: wbin2006@gmail.com)

Z. Gu is with the Cyberspace Institute of Advanced Technology, Guangzhou University, Guangzhou 510006, China. (e-mail: zqgu@gzhu.edu.cn)

X. Ling and C. Wu are with the College of Computer Science and Technology, Zhejiang University, Hangzhou 310058, China. (e-mail: lingxiang@zju.edu.cn, wuchunming@zju.edu.cn)

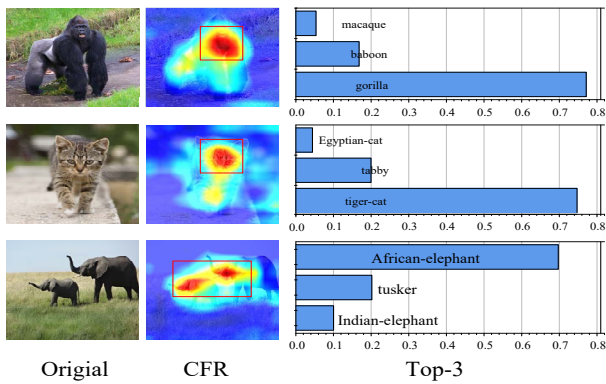


Fig. 1. Some CFR examples generated by Grad-CAM.

the perturbation magnitude of their patches and stickers is not constrained, while our method limits the perturbation within a tiny bound to be imperceptible to human eyes.

Although our work seems to consider CFRs at the image semantic level, it is different from image semantic segmentation [22] since our method is put more attention on the regions that impact classification while image segmentation is an attempt to find the object edge. In other words, we start from the network explanation while image segmentation focuses on the object itself. Recently, C. Xie et al. [23] craft adversarial examples to fool semantic segmentation and object detection, while Z. Gu et al. [24] leverage the YOLO detector to locate sensitive regions for adding perturbations. Essentially, their methods do not fully utilize the network explanation. Besides, the size of our CFR is far smaller than the region obtained by object detectors.

The main innovations and contributes to our work can be summarized as follows:

- To the best of our knowledge, we are the first to utilize network explanations to create adversarial patches at the semantic level. This method combines network explanations and optimization techniques to achieve a good tradeoff between strength and imperceptibility. As a result, we improved the adversarial patch method in two aspects. First, the magnitude of perturbations is substantially reduced, which is almost imperceptible to humans. Second, the position of the adversarial patch is determined at the semantic level.
- We confirmed the reasonable explanation of Grad-CAM through adversarial examples. Our work shows that the adversarial perturbations added to the CFR located by network explanations can effectively fool CNNs. It reveals an important fact that CNN has some characteristics of human neural networks from a novel perspective, that is, the CNN has an attention mechanism similar to humans to some extent, which provides a crucial clue for the further exploration of artificial intelligence.
- Extensive experiments are conducted on CIFAR-10 and ILSVRC2012, which demonstrate that CFRs patch attack consistently outperforms state-of-the-art methods in the attack success rate despite in white-box or black-box settings. In brief, compared with the recent proposed patch attacks, the patch crafted by our method is imperceptible;

compared with the global attacks, the magnitude of our perturbations is the smallest.

The rest of the paper is organized as follows. The next section highlights the related works in various adversarial attacks, including global perturbations and local perturbations at pixel levels. Then we describe our method to craft perturbations on CFRs in Section III, and the experimental results in Section IV. Finally, we conclude the paper in Section V.

## II. RELATED WORK

In this section, we introduce some related works on adversarial attacks according to the perturbed regions. These attacks are classified into global adversarial attacks and local adversarial attacks. Our approach proposed in this paper belongs to the latter. However, different from previous local attacks at the pixel level, we add perturbations on some semantic regions through network explanations. The global adversarial attacks at the pixel level are introduced in Section II-A, and the local adversarial attacks at the pixel level are presented in Section II-B.

### A. Global Adversarial Attacks at Pixel Levels

C. Szegedy et al. [7] first found that DNNs are vulnerable to adversarial examples, they proposed a box-constrained optimal perturbation method called L-BFGS. Since L-BFGS used an expensive linear search method to find the optimal perturbation, it was time-consuming and impractical. I. J. Goodfellow et al. [8] proposed FGSM (Fast Gradient Sign Method) to generate adversarial examples. They only performed a one-step gradient update along the direction of the sign of gradient at each pixel, so the computation cost is extremely lower. However, the generated adversarial example may not perform the best. According to [9], a one-step attack like FGSM is easy to transfer but also easy to defend. Based on FGSM, many other improved methods are proposed, such as I-FGSM proposed by A. Kurakin et al. [25], in which momentum is applied to FGSM to generate adversarial examples more iteratively. F. Tramèr et al. [26] found that FGSM with adversarial training is more robust to white-box attacks than black-box attacks due to gradient masking. They proposed a RAND-FGSM, which added random noise when updating the adversarial examples to defeat adversarial training. Y. Dong et al. [27] proposed MI-FGSM that assumed the gradients at each iteration are related to not only the current gradients but also the gradients in the previous iteration. More recently, M-DI<sup>2</sup>-FGSM [28] based on MI-FGSM is proposed to improve transferability in black-box attacks.

Besides these FGSM series of attacks, the researchers have proposed a variety of other improved algorithms. S.-M. Moosavi-Dezfooli et al. [29] proposed Deepfool to find the closest distance from the original input to the decision boundary of adversarial examples. To overcome the non-linearity in a high dimension, they performed an iterative attack with a linear approximation. DeepFool provided less perturbation compared to FGSM. N. Carlini and D. Wagner [11] proposed the C&W method to defeat defensive distillation. C&W considers three forms of perturbation constraints

( $\ell_0$ ,  $\ell_1$  and  $\ell_\infty$  norm of the added perturbations) and adjusts the added perturbations with the optimization method. As far as we know, C&W is one of the most powerful attacks at the pixel level. All of these works achieve some significant progress; however, they do not fully take into account the semantic of images, which will bring more redundant perturbations to pixels.

### B. Local Adversarial Attacks at Pixel Levels

Different from manipulating each image pixel for misclassification, several methods are proposed to perturb some pixels, which are called local adversarial attacks in this paper. A classic method is JSMA proposed by N. Papernot et al. [17] for targeted attacks. They perturbed a small number of pixels by a constant offset in each iteration step that maximizes the saliency map. However, JSMA has the disadvantage of over-modifying the value of the pixels, making the added perturbations easily perceptible by the naked eye, and its adversarial strength is weak [30]. J. Su et al. [18] proposed a one-pixel attack method that successfully deceives the DNNs by modifying the value of a single pixel. Although this method is better for low-resolution images (such as CIFAR-10), the attack success rate for high-resolution images will be greatly reduced (such as ImageNet), and the cost is very large  $\ell_1$  distortion [31].

The pixels perturbed by JSMA are usually nonadjacent, another kind of method manipulates the pixels in a continuous region. I. Evtimov et al. [21] proposed a sticker attack that added noise patches as rectangular patterns on top of traffic signs to cause misclassification. T. B. Brown et al. [19] present a method to create universal, robust, targeted adversarial image patches in the real world. Our method different from them exists in three aspects. First, the size of the patch in Adversarial Patch is determined manually while it in our method is determined by the CFRs automatically. Second, the patch location of Adversarial Patch can be random in the image, while the position in our method is through Grad-CAM at the semantic level. Finally, the patches are obvious in Adversarial Patch, while our patches are imperceptible. D. Karmon et al. [20] generate localized adversarial noises that cover only 2% of the pixels in the image, none of them over the main object, and that is transferable across images and locations, and successfully fool a state-of-the-art Inception v3 model with very high success rates. Although these stickers and patch attacks have demonstrated high strength and can easily bypass existing defense approaches, there is no constraint on noise and they are obvious to be observed easily. Moreover, the location of stickers or patches is randomly determined by the adversary. Z. Gu et al. [24] leverage the YOLO detector to locate sensitive regions for adding perturbations. In contrast, the goal of our method is to locate a sensitive region through network explanations and add imperceptible perturbations.

## III. METHODOLOGY

A CNN can be generally expressed as a mapping function  $f(X, \theta) : \mathbb{R}^m \rightarrow \mathbb{R}^C$ , where  $X \in \mathbb{R}^m$  is an input variable,  $\theta$  denotes all the parameters and  $C$  is the number

of classes. Typically, CNN is comprised of convolutional layers with some method of periodic downsampling (either through pooling or stride convolutions). Let  $Z$  be the output vector of the penultimate layer, namely the Logits layer. This defines a mapping function:  $X \mapsto Z$ . The last layer of the CNN is the softmax layer. Then the softmax function can be expressed as  $S(Z)_j = \exp(Z_j) / \sum_{i=1}^C \exp(Z_i)$ , where  $Z_i$  is the  $i$ -th element of  $Z$ , and  $i \in [C]$ ,  $[C] = \{1, \dots, C\}$ . Thus the final model can be expressed as  $f(X) = S(W_s Z + b_s)$ , where  $W_s$  and  $b_s$  are the weight matrix and bias vector of the softmax layer respectively. Given an input  $X$  with the ground-truth class  $y$ , the predicted class of  $X$  can be expressed as  $\hat{y} = \arg \max_{i \in [C]} f(X)_i$ . An adversarial example can be represented as  $X' = X + \delta$ , where  $X$  is a clean nature image, and  $\delta$  is the perturbation. For obtaining imperceptible perturbations,  $\delta$  is always constrained by a  $p$ -norm,  $\|\delta\|_p \leq \epsilon$ , where  $p = \ell_0, \ell_2$  or  $\ell_\infty$  and  $\epsilon$  is the perturbation bound.

Inspired by the ‘‘attention mechanism’’ [32], we believe that not each region in an image makes the same contribution to the classification of CNNs. Therefore, if we find a sensitive region for classification and add perturbations to them, it will be more effective to fool the classifier with fewer perturbations than previous methods [33]. Although the intrinsic mechanisms of CNNs are not fully understood by humans, some recent works have demonstrated more interesting clues [15], [14], [34]. These state-of-the-art explanations inspire us to craft local region perturbations in an interpretable way.

### A. Thread Models

In general, the method to generate adversarial examples needs some proper assumptions. These assumptions consist of a so-called thread model. X. Yuan et al. [35] presented a deep learning threat model in two dimensions. The first dimension is the adversarial goal including *targeted attacks* and *untargeted attacks* according to the adversarial specificity. The second dimension is the attacker ability defined by the amount of information that the attacker can obtain from target CNNs, which are divided into two categories, i.e., *white-box attacks* and *black-box attacks*.

**Adversarial Goal:** For untargeted attacks, the adversarial example  $X'$  satisfies  $y' \neq y$ , i.e.,  $y'$  can be any class except  $y$  (the ground truth label of  $X$ ), where  $y' = \arg \max_{i \in [C]} f(X')_i$ . For targeted attacks, we specify a target class  $y^*$ , and the adversarial example  $X'$  must satisfy  $y^* = \arg \max_{i \in [C]} f(X')_i$  and  $y^* \neq y$ . In this paper, we mainly focus on untargeted attacks that are suitable for further adversarial training.

**Adversarial Capabilities** are defined by the amount of information that the adversary has about the target classifier. The so-called white-box attack means that the adversary has almost all the information on the target CNN, including training data, activation functions, network topologies, and so on. The black-box attack, however, assumes the attacker has no way to access the internal information of the trained neural network model, except the output of the model including the label and confidence. In this paper, we assume white-box settings like FGSM, C&W, etc. Nevertheless, all white-box attacks can be employed to lunch black-box attacks employing a substitute model as described in [36].

### B. Problem Formulation

In this paper, we want to add perturbations to a local region instead of on a whole image. To formalize the problem of patch attacks, let  $X_r$  denote the region to add the perturbation  $\delta_r$ . Note that  $X_r$  is generally not a regular region while  $X$  is a rectangular. For conveniently computing, we introduce a binary matrix  $M$  to represent the shape of  $X_r$ . Here  $M$  is a 0-1 matrix:

$$M(i, j) = \begin{cases} 1 & X(i, j) \in X_r \\ 0 & \text{otherwise} \end{cases} \quad (1)$$

where  $X(i, j)$  is a pixel at the cell  $(i, j)$  of  $X$ . Thus we can transfer  $X_r$  to a matrix by  $X \odot M$ , where  $\odot$  is the Hadamard product. Accordingly,  $\delta_r$  can be represented by matrix form  $\delta \odot M$ , where  $\delta$  is a global perturbation. Thus, obtaining an optimal  $\delta_r$  can be modeled as the following constrained optimization problem:

$$\begin{aligned} \min \quad & \|\delta \odot M\|_p \\ \text{s.t.} \quad & f(X + \delta \odot M) \neq y \\ & X + \delta \odot M \in [0, 1]^m \end{aligned} \quad (2)$$

Problem (2) can be very difficult to solve, however, we instead solve the following problem:

$$\begin{aligned} \max \quad & J(X + \delta \odot M, y) \\ \text{s.t.} \quad & X + \delta \odot M \in [0, 1]^m \end{aligned} \quad (3)$$

where  $J$  is a loss function. We think solving this problem lies in two key points. The one is to locate  $X_r$ , i.e., identifying the binary matrix  $M$ , as described in Section III-C; the other is to find a proper loss function to solve problem (3), as demonstrated in Section III-D.

### C. Contributing Feature Regions (CFRs)

Suppose the input image  $X \in \mathbb{R}^m$  is forward propagated through the CNN, and the final convolutional layer outputs the high-level feature map  $A$  of the image, where  $A^{(k)} \in \mathbb{R}^{u \times v}$  represents feature map of the  $k$ -th convolutional kernel with the size of  $u \times v$ . Next,  $A$  passing through the fully connected layers and finally outputs a confidence vector  $Z$ . Let  $Z_c$  represent the logits value of the  $c$ -th class. A larger value of  $Z_c$  indicates the  $X$  is predicted to the  $c$ -th class with a greater probability. To this end, we compute the gradient of  $Z_c$  with respect to  $A^{(k)}$ , i.e.,  $\partial Z_c / \partial A^{(k)}$  to measure the classification prediction importance of the  $k$ -th convolutional kernel to the  $c$ -th class. Furthermore, we adopt the global average pooling operation to calculate the weight  $\lambda_c^{(k)}$  of the  $k$ -th convolutional kernel:

$$\lambda_c^{(k)} = \frac{1}{u \times v} \sum_p \sum_q \frac{\partial Z_c}{\partial A_{pq}^{(k)}} \quad (4)$$

where  $A_{pq}^{(k)}$  is the activation at the cell  $(p, q)$  of the  $k$ -th convolutional kernel. Thus, we obtain a feature activation map  $\sum_k \lambda_c^{(k)} A^{(k)}$  for the  $c$ -th class. Considering that only the positive elements in  $\sum_k \lambda_c^{(k)} A^{(k)}$  have a positive effect on the classification, the result is further reactivated by ReLU

to remove the influence of negative elements, and the final activation map of the  $c$ -th class is obtained:

$$L_c = \text{ReLU} \left( \sum_k \lambda_c^{(k)} A^{(k)} \right) \quad (5)$$

In fact, in our work the  $c$ -th class is the ground-truth class  $y$  of  $X$ . In the following, we substitute  $y$  for  $c$ . We visualize  $L_y$  in the form of a heatmap (e.g. Fig. 1), in which the red regions represent CFRs of the class  $y$ . For further distinguishing the contribution of each pixel in the CFRs, we design a soft-mask  $\tilde{M}$  instead of the traditional binary mask in Eq. (1).

$$\tilde{M}(i, j) = \begin{cases} \frac{L_y(i, j)}{\sum_{m, n} L_y(m, n)} & L_y(i, j) \geq \tau, L_y(m, n) \geq \tau \\ 0 & \text{otherwise} \end{cases} \quad (6)$$

where  $\tau$  is a threshold. The detail to obtain the perturbation  $\delta_{CFR}$  is illustrated in Algorithm 1.

### D. Generate Perturbations for CFRs

After locating the CFR, we further generate the local perturbation  $\delta_{CFR}$  on the CFR. We design a new loss function to implement problem (3), which consists of two parts: (1) a cross-entropy loss function  $J_{CE}$  for generating adversarial examples, and (2) an  $\ell_2$  regularization function to limit the perturbation. In theory, the  $\ell_0$  and  $\ell_\infty$  can also be used for regularization. However, we notice that the  $\ell_0$  norm is non-differentiable and hard for the standard gradient descent algorithm. Also, the  $\ell_\infty$  norm only focuses on the largest value in  $\delta_{CFR}$ , it easily oscillates between two sub-optimal solutions during the gradient descent process [11].

$$J = J_{CE} + \beta \frac{1}{\|\delta \odot \tilde{M}\|_2} \quad (7)$$

where  $\beta$  is a hyper-parameter to control the degree of distortion (we set  $\beta = 1$ ) and  $\delta \odot \tilde{M}$  represents  $\delta_{CFR}$ .

Remind the original cross-entropy loss function is  $J_{CE} = -\log S_y$ , where  $S_y = \exp(Z_y) / \sum_{i=1}^C \exp(Z_i)$ . In adversarial settings, we aim to maximize  $J_{CE}$  for obtaining an optimal adversarial example. However, when  $S_y$  tends to approach 1,  $J_{CE}$  is close to 0. Thus, the update of  $\delta_{CFR}$  has minimal impact on  $J_{adv}$ , which is undesirable to us. To avoid this situation, we introduce a hyper-parameter  $T$  ( $T > 0$ ) called *inverse temperature* inspired by the distillation idea [16]. Then  $J_{CE}$  is modified as follows:

$$J'_{CE} = \frac{-\log(S_y)}{T} \quad (8)$$

where  $S_y \in (0, 1)$  and  $\log(S_y) \in (-\infty, 0)$ . If  $0 < T < 1$ , the lower bound of  $\log(S_y)/T$  is magnified and  $-\log(S_y)/T$  becomes larger, that is,  $J'_{CE}$  becomes larger. If  $T > 1$ , the lower bound of  $\log(S_y)/T$  is reduced and  $-\log(S_y)/T$  becomes smaller, that is,  $J'_{CE}$  gets smaller. Our goal is to maximize  $J'_{CE}$ , so we set  $0 < T < 1$ .

Since maximizing  $J$  are equivalent to minimizing  $1/J$ , we present the optimization problem of (7) in a standard form:

$$\begin{aligned} \min \quad & \frac{1}{J'_{CE} + \beta \frac{1}{\|\delta \odot \tilde{M}\|_2}} \\ \text{s.t.} \quad & X + \delta \odot \tilde{M} \in [0, 1]^m \end{aligned} \quad (9)$$

Finally, we use the SGD algorithm to solve problem (9).

---

**Algorithm 1** Crafting Adversarial Patch Examples
 

---

**Input:** A clean image  $(X, y)$ ; the iterations  $N$ ; the step size  $\eta$ ; the degree of distortion  $\beta$ ; the threshold  $\tau$ ; the inverse temperature  $T$

**Output:**  $X'$

- 1: initialize  $\delta$   
 //  $K$  is the number of feature maps in the last layer of convolution layers
  - 2:  $\lambda_y^{(k)} \leftarrow \frac{1}{u \times v} \sum_p \sum_q \frac{\partial Z_y}{\partial A_{pq}^{(k)}}$ ,  $k = 1, \dots, K$
  - 3:  $L_y \leftarrow \text{ReLU} \left( \sum_k \lambda_y^{(k)} A^{(k)} \right)$   
 // Get CFRs
  - 4:  $\tilde{M}(i, j) = \begin{cases} \frac{L_y(i, j)}{\sum_m \sum_n L_y(m, n)} & L_y(i, j) \geq \tau, L_y(m, n) \geq \tau \\ 0 & \text{others} \end{cases}$
  - 5: **for**  $i = 1 \dots N$  **do**
  - 6:      $X' \leftarrow X + \delta \odot \tilde{M}$
  - 7:      $J \leftarrow \left( J'_{CE} + \beta \frac{1}{\|\delta \odot \tilde{M}\|_2} \right)$   
 // Update  $\delta$
  - 8:      $\delta \leftarrow (\delta - \nabla_{\delta} (1/J) \times \eta) \odot \tilde{M}$
  - 9: **end for**
- 

#### IV. EXPERIMENTS

In this section, we first describe the datasets, models, and metrics used in our experiment. Then we show the impact of CFRs on classification by simply setting the CFR to 0. The results confirm that the CFR play a critical role in classification. For intuition, we visualizing the adversarial examples and their perturbation of various methods. In white-box settings, we compare the ASR, SSIM, and  $\ell_p$  of our method with the classic global attacks such as PGD and C&W, and local attacks such as JSMA, One-pixel. Two recent patch attacks Adversarial Patch and LaVAN are also compared. Consider the above experiments are conducted on non-protected models, we further explore the effect of our method on protected models. Besides, we compare the transferability of our method with other attacks in black-box settings. Finally, several key hyper-parameters are discussed.

##### A. Experiment Setup

**Datasets and Models.** We validate our method on two benchmark datasets CIFAR-10 [37] and ILSVRC2012 [38]. CIFAR-10 consists of 60,000 images with the size of  $32 \times 32$ , including 10 categories and each with 6,000 images, in which 50,000 images are used for training and 10,000 images are used for tests. ILSVRC2012 contains 1,000 categories, in which 1,200 thousand images are used for training, and 50,000 images are used for tests. All the images we use to generate adversarial examples are correctly classified by all

models, which can guarantee all the misclassified examples are adversarial examples. Two popular CNNs VGG [2] and ResNet [3] are selected for our experiment. According their layers, they are further divided into VGG-11, VGG-13, VGG-16, ResNet-18, ResNet-34, and ResNet-50.

**Evaluation Metrics.** We use (1) the attack success rate (ASR) to measure the power of the adversarial examples, (2) the  $\ell_p$  norm to measure the perturbation amplitude, and (3) the structural similarity (SSIM) index as a measurement of image similarity because human visual perception is highly sensitive to the structural information of an image [39].

(1) **ASR:** Given  $n$  clean images correctly classified by the CNN, the corresponding adversarial examples are obtained by a special generating method. Suppose  $X_i$  represents the  $i$ -th clean image, its true label is  $Y_i$ , and  $X'_i$  is its corresponding adversarial image. Then ASR can be obtained by the following formula:

$$\text{ASR} = 100 \times \frac{1}{n} \sum_{i=1}^n r \quad (10)$$

$$\text{where } r = \begin{cases} 1, \arg \max f(X'_i) \neq Y_i \\ 0, \arg \max f(X'_i) = Y_i \end{cases}.$$

(2) **SSIM:** Given a clean image  $X$  and its corresponding adversarial image  $X'$ ,  $\text{SSTM}(X, X')$  measures the similarity between  $X$  and  $X'$ . A larger  $\text{SSTM}(X, X')$  indicates a higher similarity between two images.

$$\text{SSIM}(X, X') = [l(X, X')]^\alpha [c(X, X')]^\beta [s(X, X')]^\gamma \quad (11)$$

where  $\alpha, \beta, \gamma > 0$ ,  $l(X, X')$  is brightness comparison,  $c(X, X')$  is contrast comparison and  $s(X, X')$  is structure comparison:

$$l(X, X') = \frac{2\mu_X \mu_{X'} + c_1}{\mu_X^2 + \mu_{X'}^2 + c_1} \quad (12)$$

$$c(X, X') = \frac{2\sigma_{XX'} + c_2}{\sigma_X^2 + \sigma_{X'}^2 + c_2} \quad (13)$$

$$s(X, X') = \frac{\sigma_{XX'} + c_3}{\sigma_X \sigma_{X'} + c_3} \quad (14)$$

where  $\mu_X$  and  $\mu_{X'}$  represent the average of  $X$  and  $X'$  respectively;  $\sigma_X$  and  $\sigma_{X'}$  represent the standard deviation of  $X$  and  $X'$  respectively,  $\sigma_{XX'}$  represents the covariance of  $X$  and  $X'$ ;  $c_1, c_2$ , and  $c_3$  are constants.

##### B. Impact of CFRs on Classification

We first evaluate the impact of CFRs on the classifier through two groups of special adversarial images. The image in one group keeps the pixels in CFR unchanged while the rest of the pixels are set to 0, which is denoted as Adv-non-CFR. On the contrary, the image in the other group keeps the pixels unchanged other than the CFR that is set to 0, which is denoted as Adv-CFR. These special adversarial images are crafted from 10,000 clean images on CIFAR-10 and adopted the threshold  $t = 0.2$ . Fig. 2 shows the examples of Adv-CFR and Adv-non-CFR. These examples of Adv-CFR and

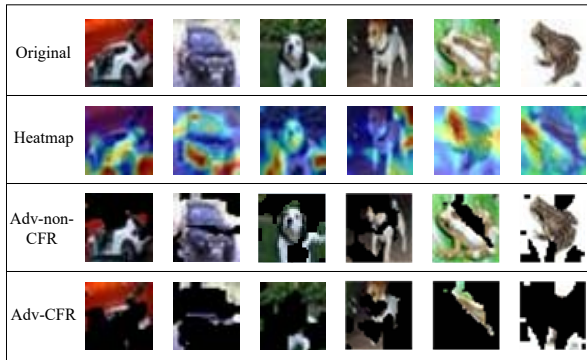


Fig. 2. Two groups of special adversarial images: Adv-CFR and Adv-non-CFR.

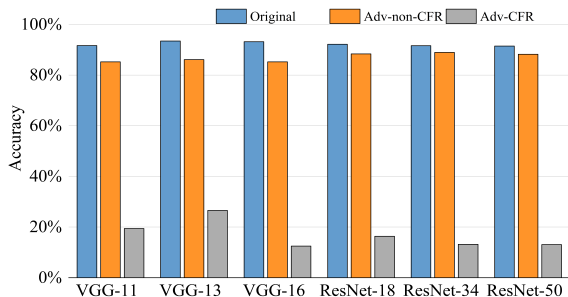


Fig. 3. Accuracy of different models with clean images, Adv-CFR, and Adv-non-CFR examples

Adv-non-CFR are tested on VGG and ResNet, and the results are shown in Fig. 3. Compare to the original clean images, the accuracy of Adv-non-CFR decreases by no more than 3%, however, the accuracy of Adv-CFR decreases by at least 60%. The result reconfirms the conclusion of Grad-CAM that the CFRs play a key role in the classification.

### C. Visualizing Adversarial Attacks

To intuitively perceive adversarial examples and the added perturbations, we present them in Fig. 4, 5, and 6. PGD and C&W adversarial examples belong to global pixel perturbations, which are compared with our method on CIFAR-10 (see Fig. 4) and ILSVRC2012 (see Fig. 5). It can be seen that the images added by our patch perturbations are perfectly closer to the original clean images than these global perturbed images. On CIFAR-10, the average SSIM of PGD is 0.94, C&W is 0.94, while our method is 0.99. On ILSVRC2012, the average SSIM of PGD is 0.91, C&W is 0.89, while our method is 0.99.

Two recent patch attack methods—Adversarial Patch [19] and LaVAN [20] are compared with our method on ILSVRC2012. In particular, due to the low resolution and relatively small of CIFAR-10, this method does not use it. For Adversarial Patch, we use the same experimental setting as [19] attacking 15% of image size. For LaVAN, we follow the same implementation as [20] that adversarial patches cover 2% pixels in the image. Fig. 6 presents the patches, adversarial examples, and the SSIM value of two methods. This can be further confirmed by the SSIM value, where our method is perfectly close to 1 under the same  $\ell_2$  norm constraint.

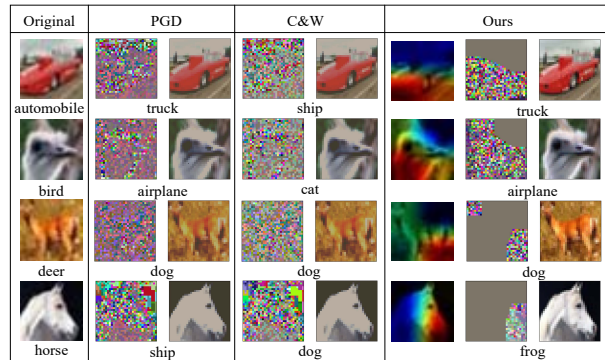


Fig. 4. Comparison of perturbations and adversarial examples generated by PGD, C&W, and our method on CIFAR-10 (all these three methods are constrained by  $\ell_2 = 2$ ).

### D. Comparison among Adversarial Attacks

To further illustrate the superior performance of our method, we report the ASR, SSIM, and  $\ell_p$  distortion of different attack methods in Table I. ResNet-18 and VGG-19 are leveraged to run on CIFAR-10 and ILSVRC2012 respectively. Six classic adversarial attack methods are compared with our method. For PGD, the perturbation bound  $\epsilon = 16$ , the step size  $\alpha = 2$ , and 20 iterations are adopted. For C&W, the constant  $c = 1$ , learning rate  $lr = 0.01$  and 1,000 iterations are adopted. Besides the global attacks PGD and C&W, two local attacks JSMA and one-pixel attack are also considered. For JSMA, we set intensity variations  $\theta = 0.3$ . For a one-pixel attack, we adopt five pixel-modification. For Adversarial Patch (non-target), we still attack 15% of image size. For LaVAN (non-target), we train the noise up to 10,000 iterations, perturb roughly 2% of the image pixels and choose the location around the corners.

Specifically, besides our CFR patch attack, PGD and C&W have the high ASR while have the larger distortion, i.e., the larger  $\ell_p$  ( $p = 0, 1, 2, or \infty$ ) and the smaller SSIM on CIFAR-10 and ILSVRC2012. Compare to our method, JSMA is lower with ASR (ASR: 90.33% vs. 100.00%); and larger with  $\ell_p$  distortion on CIFAR-10. On ILSVRC2012, our method still outperforms JSMA. In particular, the  $\ell_1$  distortion of JSMA reaches the maximum value of 1, which means that the human eyes can easily distinguish the modified pixel. For the one-pixel attack, we choose to attack 5 pixels. Although the  $\ell_0$  and  $\ell_1$  distortion of the one-pixel attack is smaller than our method on CIFAR-10, the  $\ell_2$  and  $\ell_\infty$  distortion is greater than our method. Furthermore, the ASR of the one-pixel attack is only 80.77%, which is far lower than that of ours (100%). On ILSVRC2012, the  $\ell_0$ ,  $\ell_1$  and  $\ell_2$  distortion of the one-pixel attack are the smallest, but the  $\ell_\infty$  distortion also reaches the maximum value of 1 and its ASR is only 40.56%. Compared with Adversarial Patch and LaVAN, although the  $\ell_0$  distortion smaller than our method, the  $\ell_2$  and  $\ell_\infty$  distortion are far greater than our method and the patch is clearly visible to the human eye. In summary, our method achieves the most powerful attack ability, besides it can ensure the perturbations imperceptibly.

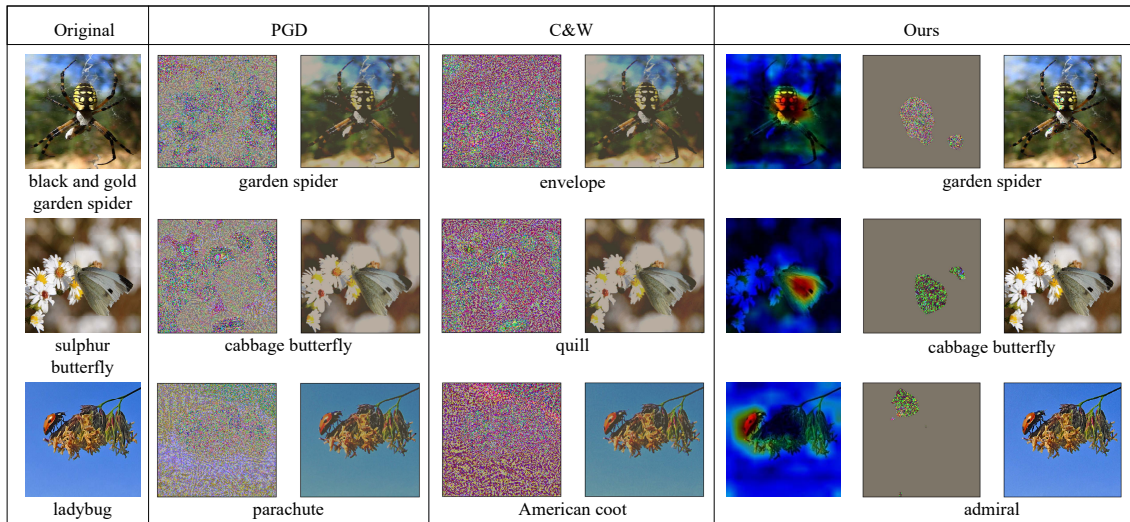


Fig. 5. Comparison of perturbations and adversarial examples generated by PGD, C&W, and our method on ILSVRC2012 (all these three methods are constrained by  $\ell_2 = 45$ ).

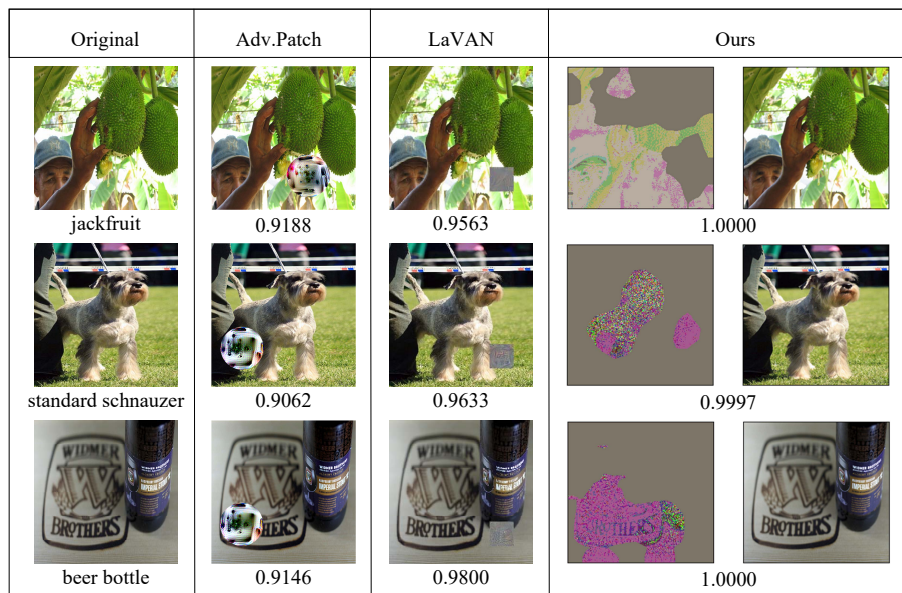


Fig. 6. SSIMs of three patch attacks on ILSVRC2012. The penultimate row visualizes the patch perturbation generated by our method.

TABLE I  
ASR, SSIM, AND  $\ell_p$  DISTORTION FOR VARIOUS ATTACKS

Dataset	Attack Methods	ASR	SSIM	$\ell_0$	$\ell_1$	$\ell_2$	$\ell_\infty$
CIFAR-10	PGD	93.18%	0.94	3,060	265.84	5.57	0.16
	C&W	97.44%	0.94	2,832	797.97	21.01	0.94
	JSMA	90.33%	0.71	335	856.11	28.04	1.00
	One-pixel	80.77%	0.99	15	24.89	7.03	1.00
	Ours	100.00%	0.99	2,333	77.03	1.56	0.07
ILSVRC2012	PGD	97.70%	0.91	150,528	138,318.30	373.95	0.93
	C&W	99.33%	0.89	150,528	114,239.05	297.80	0.98
	JSMA	90.00%	0.94	447	75,375.33	194.35	1.00
	One-pixel	40.56%	0.99	15	29.43	8.69	1.00
	Adversarial Patch	99.48%	0.90	14,700	16,684.98	163.20	1.00
	LaVAN	95.10%	0.96	7,500	5,985.29	73.53	1.00
Ours	100.00%	0.99	98,431	7,835.55	42.94	0.28	

### E. Transferability

Transferability is a well-known property of adversarial examples, that is, the adversarial examples misleading one model can also mislead other models [40]. This property is generally utilized by the adversary to launch a black-box attack. In this section, we compare the transferability of our CFR patch examples with other classic adversarial examples in black-box settings. In these methods, PGD, M-DI<sup>2</sup>-FGSM, and C&W are global adversarial attacks, while Adversarial Patch and LaVAN are local adversarial attacks. Note the model for crafting adversarial examples is referred to a *substitute model*, while the model for testing adversarial examples is termed as a *target model* in this paper.

For CIFAR-10, we choose VGG-11, VGG-13, VGG-16, ResNet-18, and ResNet-34 as target models, and one of them as a substitute model. Then we obtain five heatmaps as shown in Fig. 7 (a)-(e), where the horizontal axis represents the adversarial examples (i.e., PGD, M-DI<sup>2</sup>-FGSM, etc.) generated on one substitute model, and the vertical axis represents the target models. The element in the heatmap is the accuracy of target models against adversarial examples, in which smaller values indicate higher transferability. Note when the substitute model is consistent with the target model, it is equivalent to a white-box attack. Therefore, in this case, the accuracy will be very lower than other target models. Here we focus on transferability and merely consider the case that the target model is different from the substitute model. In Fig. 7, we observed that the adversarial examples generated with our method have higher transferability than other attack methods, including state-of-the-art M-DI<sup>2</sup>-FGSM. The same conclusion is obtained with ILSVRC2012 in Fig. 8, which indicates perturbation crafted with network explanations has more powerful attack ability in black-box settings.

### F. Adversarial Attacks on Protected Models

The above foregoing evaluation is conduct on the target model without protection. Now we further test the attack ability of our patch adversarial examples on the protected model. We mainly focus on the model protected by adversarial training, because adversarial training is popularly considered as one of the most effective defenses. Here we use Fast adversarial training [41] and PGD adversarial training [10]. For Fast adversarial training, we set the perturbation bound  $\epsilon = 8$  on CIFAR-10 and  $\epsilon = 2$  on ILSVRC2012 respectively. For PGD adversarial training, we set 7 iteration steps, the step size  $\alpha = 2$ , and the total perturbation bound  $\epsilon = 8$ . Finally, we obtain four protected models ResNet-18-Fast, ResNet-18-PGD, VGG-16-Fast, and VGG-16-PGD.

Consider the image size of CIFAR-10 is too small, we only conduct patch attacks on ILSVRC2012. For CIFAR-10, we compare PGD, C&W, and our method. For ILSVRC2012, we add two patch attacks Adversarial Patch and LaVAN. Table II reports the results of the protected models under various attacks. We observe that adversarial training cannot achieve perfect performance against these attacks (the ASR higher than 50.00%). Among them, our CFR patch attack outperforms

TABLE II  
ATTACK THE ADVERSARIAL TRAINING MODEL

Dataset	Protected Models	Attack Methods	ASR
CIFAR-10	ResNet-18-Fast	PGD	63.66%
		C&W	70.79%
		Ours	79.00%
	ResNet-18-PGD	PGD	57.57%
		C&W	65.71%
		Ours	77.39%
ILSVRC2012	VGG-16-Fast	PGD	65.99%
		C&W	66.11%
		Adversarial Patch	63.89%
	VGG-16-PGD	LaVAN	67.11%
		Ours	79.87%
		PGD	63.50%
	VGG-16-PGD	C&W	57.72%
		Adversarial Patch	75.75%
		LaVAN	65.00%
		Ours	77.60%

other attacks in ASR. For example, our method can achieve 79.87% ASR against VGG-16-Fast on ILSVRC2012.

### G. Analysis of Hyper-Parameters

**Iterations  $N$  and inverse temperature  $T$**  are two dominant hyper-parameters in our algorithm, and here we focus on their effects on ASR. We observe that ASR tends to increase along with increases in Fig. 9. When  $N=30$ , ASR of our method can reach 100% on both datasets with a proper inverse temperature (e.g.  $T=0.1$ ), which indicates that our objective function can find the global optimal solution with fine-tuned parameters. We further discuss the impact of inverse temperature  $T$ . As shown in Fig. 9, when  $T > 1$  or  $T$  is too small, it will prevent our patch attack from achieving a higher ASR regardless of increasing iterations. Remind that the purpose of inverse temperature  $T$  is to prevent the loss  $J_{adv}^T$  from decreasing to 0 as shown in Section III-D. Nevertheless, when  $T > 1$ ,  $J_{adv}^T$  becomes smaller, which leads to a smaller ASR, e.g., when  $T = 2$ , it achieves the lowest ASR in Fig. 9. Similarly, the smaller  $T$  makes  $J_{adv}^T$  become so large that it deviates far from the original value and the optimal direction, which makes it hard to converge to the optimal solution. For instance, when  $T < 0.1$ , the ASR of patch attacks present a downward trend. In summary, a moderate value of  $T$  is desirable, e.g.,  $T = 0.1$  for ILSVRC2012.

**Threshold  $\tau$**  is also a dominant hyper-parameter to determines the shape of CFRs, that is, the size of the range of adding perturbations. We use  $\ell_0$  norm to measure the number of perturbed pixels. Specifically,  $\tau = 0$  means the total pixels in the image are perturbed. As shown in Fig. 10, ASR and  $\ell_0$  are presented in the same figure with two independent vertical axes. We observe that increasing the threshold  $\tau$  can decrease  $\ell_0$  norm, i.e., the size of perturbed regions is reduced, however, it does not affect the ASR of our patch attacks. The reason is that the most contributing pixels are maintained all the time despite the size of perturbed regions changed with  $\tau$ . In other words, it reconfirms that the classification is mainly determined by the most contributing pixels.



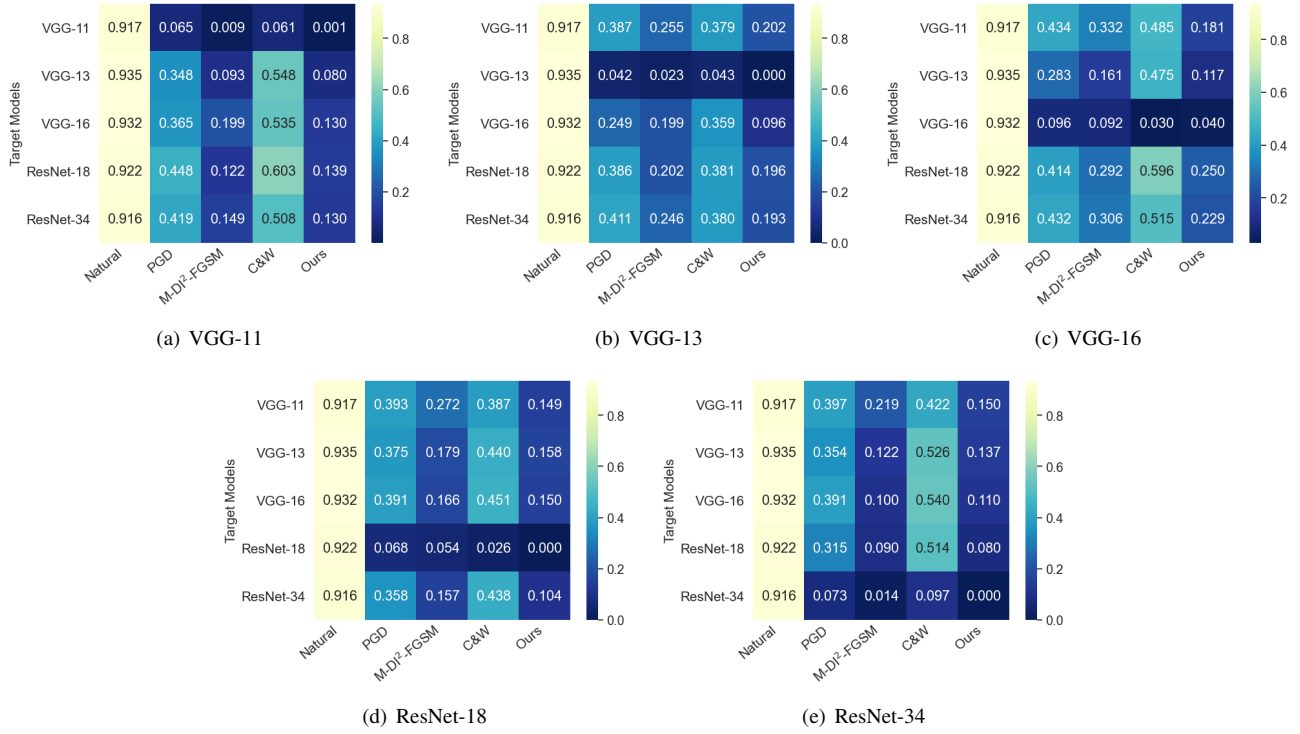


Fig. 7. Transferability on CIFAR-10, which is represented by the accuracy of the target model against the adversarial examples generated by another substitute model. The horizontal axis represents various attack methods: PGD ( $s = 20, \epsilon = 16, \alpha = 2$ ), M-DI<sup>2</sup>-FGSM ( $s = 20, \epsilon = 16, \alpha = 2, p = 0.5$ ), C&W ( $c = 1, lr = 0.01, iterations = 1,000$ ), Ours ( $\tau = 0.2, T = 0.1, \eta = 10, N = 20, \beta = 1$ ), and Natural represents the accuracy of five models on clean test examples; the vertical axis represents different models.

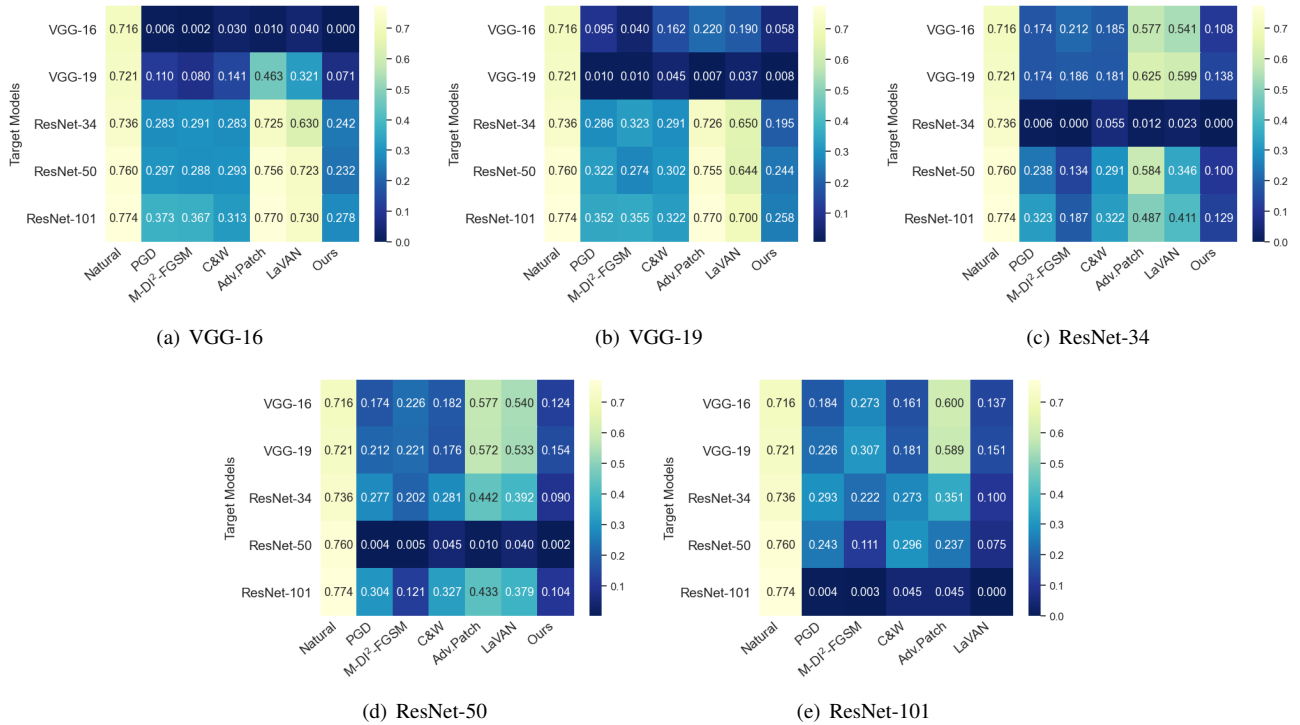
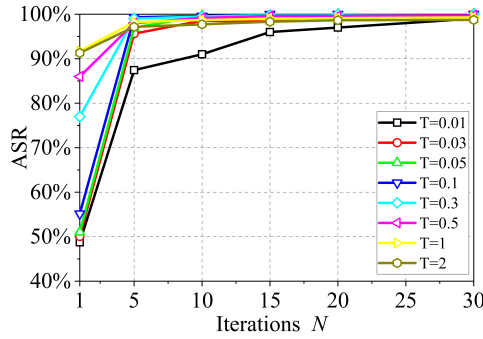
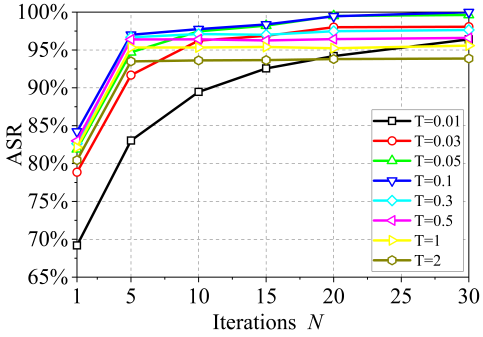


Fig. 8. Transferability on ILSVRC2012, which is represented by the accuracy of the target model against the adversarial examples generated by another substitute model. The horizontal axis represents various attack methods: PGD ( $s = 20, \epsilon = 16, \alpha = 2$ ), M-DI<sup>2</sup>-FGSM ( $s = 20, \epsilon = 16, \alpha = 2, p = 0.5$ ), C&W ( $c = 1, lr = 0.01, iterations = 1,000$ ), Adv.Patch ( $c = 1, lr = 0.01, iterations = 1,000$ ), Ours ( $\tau = 0.2, T = 0.1, \eta = 20, N = 20, \beta = 1$ ), and Natural represents the accuracy of five models on clean test examples; the vertical axis represents different models.

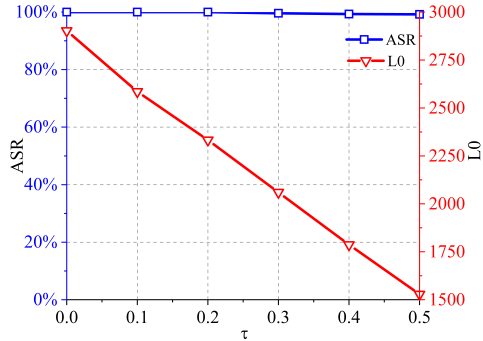


(a) CIFAR-10

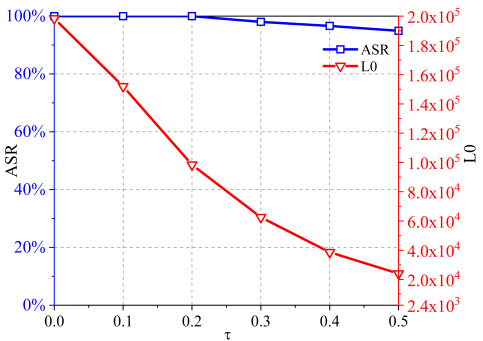


(b) ILSVRC2012

Fig. 9. The effect of iterations  $N$  and inverse temperature  $T$  on the ASR. (a) ResNet-18 network on the CIFAR-10 ( $\tau = 0.2$ ,  $\eta = 10$ ,  $\beta = 1$ ); (b) VGG-16 network on the ILSVRC2012 ( $\tau = 0.2$ ,  $\eta = 20$ ,  $\beta = 1$ ).



(a) CIFAR-10



(b) ILSVRC2012

Fig. 10. The influence of the threshold  $\tau$  on the ASR and the  $\ell_0$  norm of perturbations. (a) ResNet-18 network on CIFAR-10 ( $N = 30$ ,  $T = 0.1$ ,  $\eta = 10$ ,  $\beta = 1$ ); (b) VGG-16 network on ILSVRC2012 ( $N = 30$ ,  $T = 0.1$ ,  $\eta = 20$ ,  $\beta = 1$ ).

## V. CONCLUSIONS

This work explores a novel patch attack method by utilizing the network explanation at the semantic level. Extensive experiments on CIFAR-10 and ILSVRC2012 show that our patch attack outperforms either existing global region attacks (such as PGD and C&W) or local region attacks (such as JSMA, One-Pixel, Adversarial Patch, and LaVAN) and as well within a tiny bound to be imperceptible to human eyes. Meanwhile, the attack based on contributing feature regions may also provide a new perspective for future research on better defensive methods.

## ACKNOWLEDGMENT

This work is supported by National Key R&D Program of China (No.2018YFB2100400), Natural Science Foundation of China (No. 61972357), and Zhejiang Key R&D Program (No. 2019C03135).

## REFERENCES

- [1] A. Krizhevsky, I. Sutskever, and G. E. Hinton, "Imagenet classification with deep convolutional neural networks," *Communications of the ACM*, vol. 60, no. 6, pp. 84–90, 2017.
- [2] K. Simonyan and A. Zisserman, "Very deep convolutional networks for large-scale image recognition," *arXiv preprint arXiv:1409.1556*, 2014.
- [3] K. He, X. Zhang, S. Ren, and J. Sun, "Deep residual learning for image recognition," in *Proceedings of the IEEE Conference on Computer Vision and Pattern Recognition*, 2016, pp. 770–778.
- [4] Y. Taigman, M. Yang, M. Ranzato, and L. Wolf, "Deepface: Closing the gap to human-level performance in face verification," in *Proceedings of the IEEE Conference on Computer Vision and Pattern Recognition*, 2014, pp. 1701–1708.
- [5] J. Devlin, M.-W. Chang, K. Lee, and K. Toutanova, "Bert: Pre-training of deep bidirectional transformers for language understanding," *arXiv preprint arXiv:1810.04805*, 2018.
- [6] Y. Goldberg, "Neural network methods for natural language processing," *Synthesis Lectures on Human Language Technologies*, vol. 10, no. 1, pp. 1–309, 2017.
- [7] C. Szegedy, W. Zaremba, I. Sutskever, J. Bruna, D. Erhan, I. Goodfellow, and R. Fergus, "Intriguing properties of neural networks," *arXiv preprint arXiv:1312.6199*, 2013.
- [8] I. J. Goodfellow, J. Shlens, and C. Szegedy, "Explaining and harnessing adversarial examples," *arXiv preprint arXiv:1412.6572*, 2014.
- [9] A. Kurakin, I. Goodfellow, and S. Bengio, "Adversarial machine learning at scale," *arXiv preprint arXiv:1611.01236*, 2016.
- [10] A. Madry, A. Makelov, L. Schmidt, D. Tsipras, and A. Vladu, "Towards deep learning models resistant to adversarial attacks," *arXiv preprint arXiv:1706.06083*, 2017.
- [11] N. Carlini and D. Wagner, "Towards evaluating the robustness of neural networks," in *Proceedings of the IEEE Symposium on Security and Privacy (SP)*, 2017, pp. 39–57.
- [12] T. Tanay and L. Griffin, "A boundary tilting perspective on the phenomenon of adversarial examples," *arXiv preprint arXiv:1608.07690*, 2016.
- [13] D. Su *et al.*, "Is robustness the cost of accuracy?—a comprehensive study on the robustness of 18 deep image classification models," in *Proceedings of the European Conference on Computer Vision (ECCV)*, 2018, pp. 631–648.
- [14] B. Zhou, A. Khosla, A. Lapedriza, A. Oliva, and A. Torralba, "Learning deep features for discriminative localization," in *Proceedings of the IEEE Conference on Computer Vision and Pattern Recognition*, 2016, pp. 2921–2929.
- [15] R. R. Selvaraju, M. Cogswell, A. Das, R. Vedantam, D. Parikh, and D. Batra, "Grad-cam: Visual explanations from deep networks via gradient-based localization," in *Proceedings of the IEEE International Conference on Computer Vision*, 2017, pp. 618–626.
- [16] G. Hinton, O. Vinyals, and J. Dean, "Distilling the knowledge in a neural network," *arXiv preprint arXiv:1503.02531*, 2015.

- [17] N. Papernot, P. McDaniel, S. Jha, M. Fredrikson, Z. B. Celik, and A. Swami, "The limitations of deep learning in adversarial settings," in *2016 IEEE European Symposium on Security and Privacy (EuroS&P)*. IEEE, 2016, pp. 372–387.
- [18] J. Su, D. V. Vargas, and K. Sakurai, "One pixel attack for fooling deep neural networks," *IEEE Transactions on Evolutionary Computation*, vol. 23, no. 5, pp. 828–841, 2019.
- [19] T. B. Brown, D. Mané *et al.*, "Adversarial patch," *arXiv preprint arXiv:1712.09665*, 2017.
- [20] D. Karmon, D. Zoran, and Y. Goldberg, "Lavan: Localized and visible adversarial noise," *arXiv preprint arXiv:1801.02608*, 2018.
- [21] I. Evtimov *et al.*, "Robust physical-world attacks on machine learning models," *arXiv preprint arXiv:1707.08945*, 2017.
- [22] J. He, Z. Deng, and Y. Qiao, "Dynamic multi-scale filters for semantic segmentation," in *Proceedings of the IEEE International Conference on Computer Vision*, 2019, pp. 3562–3572.
- [23] C. Xie *et al.*, "Adversarial examples for semantic segmentation and object detection," in *Proceedings of the IEEE International Conference on Computer Vision*, 2017, pp. 1369–1378.
- [24] Z. Gu *et al.*, "Gradient shielding: Towards understanding vulnerability of deep neural networks," *IEEE Transactions on Network Science and Engineering*, 2020.
- [25] A. Kurakin, I. Goodfellow, and S. Bengio, "Adversarial examples in the physical world," *arXiv preprint arXiv:1607.02533*, 2016.
- [26] F. Tramèr, A. Kurakin, N. Papernot, I. Goodfellow, D. Boneh, and P. McDaniel, "Ensemble adversarial training: Attacks and defenses," *arXiv preprint arXiv:1705.07204*, 2017.
- [27] Y. Dong, F. Liao, T. Pang, H. Su, J. Zhu, X. Hu, and J. Li, "Boosting adversarial attacks with momentum," in *Proceedings of the IEEE Conference on Computer Vision and Pattern Recognition*, 2018, pp. 9185–9193.
- [28] C. Xie, Z. Zhang, Y. Zhou, S. Bai, J. Wang, Z. Ren, and A. L. Yuille, "Improving transferability of adversarial examples with input diversity," in *Proceedings of the IEEE Conference on Computer Vision and Pattern Recognition*, 2019, pp. 2730–2739.
- [29] S.-M. Moosavi-Dezfooli, A. Fawzi, and P. Frossard, "Deepfool: a simple and accurate method to fool deep neural networks," in *Proceedings of the IEEE Conference on Computer Vision and Pattern Recognition*, 2016, pp. 2574–2582.
- [30] N. Akhtar and A. Mian, "Threat of adversarial attacks on deep learning in computer vision: A survey," *IEEE Access*, vol. 6, pp. 14 410–14 430, 2018.
- [31] K. Xu, S. Liu, P. Zhao, P.-Y. Chen, H. Zhang, Q. Fan, D. Erdogmus, Y. Wang, and X. Lin, "Structured adversarial attack: Towards general implementation and better interpretability," *arXiv preprint arXiv:1808.01664*, 2018.
- [32] S. Zagoruyko and N. Komodakis, "Paying more attention to attention: Improving the performance of convolutional neural networks via attention transfer," *arXiv preprint arXiv:1612.03928*, 2016.
- [33] T. Deng and Z. Zeng, "Generate adversarial examples by spatially perturbing on the meaningful area," *Pattern Recognition Letters*, vol. 125, pp. 632–638, 2019.
- [34] J. Zhang, S. A. Bargal, Z. Lin, J. Brandt, X. Shen, and S. Sclaroff, "Top-down neural attention by excitation backprop," *International Journal of Computer Vision*, vol. 126, no. 10, pp. 1084–1102, 2018.
- [35] X. Yuan, P. He, Q. Zhu, and X. Li, "Adversarial examples: Attacks and defenses for deep learning," *IEEE Transactions on Neural Networks and Learning Systems*, vol. 30, no. 9, pp. 2805–2824, 2019.
- [36] N. Papernot, P. McDaniel, I. Goodfellow, S. Jha, Z. B. Celik, and A. Swami, "Practical black-box attacks against machine learning," in *Proceedings of the 2017 ACM on Asia Conference on Computer and Communications Security*, 2017, pp. 506–519.
- [37] A. Krizhevsky and G. Hinton, "Learning multiple layers of features from tiny images," *Handbook of Systemic Autoimmune Diseases*, vol. 1, no. 4, 2009.
- [38] O. Russakovsky, J. Deng, H. Su, J. Krause, S. Satheesh, S. Ma, Z. Huang, A. Karpathy, A. Khosla, M. Bernstein *et al.*, "Imagenet large scale visual recognition challenge," *International Journal of Computer Vision*, vol. 115, no. 3, pp. 211–252, 2015.
- [39] Z. Wang, A. C. Bovik, H. R. Sheikh, and E. P. Simoncelli, "Image quality assessment: from error visibility to structural similarity," *IEEE transactions on image processing*, vol. 13, no. 4, pp. 600–612, 2004.
- [40] N. Papernot, P. McDaniel, and I. Goodfellow, "Transferability in machine learning: from phenomena to black-box attacks using adversarial samples," *arXiv preprint arXiv:1605.07277*, 2016.
- [41] E. Wong, L. Rice, and J. Z. Kolter, "Fast is better than free: Revisiting adversarial training," *arXiv preprint arXiv:2001.03994*, 2020.



**Yaguan Qian** is an associate professor of School of Big-data Science, Zhejiang University of Science & Technology. He received his B.S. in Computer Science from Tianjin University in 1999, and MS and Ph.D in Computer Science from Zhejiang University in 2005 and 2014 respectively. His research interests mainly include machine learning, Big-data analysis, pattern recognition and Machine vision. In these areas he has published more than 30 papers in international journals or conferences. He is the member of CCF (China Computer Federation), CAAI (Chinese Association for Artificial Intelligence) and CAA (Chinese Association of Automation).



**Jiamin Wang** received the bachelor's degree from Zhejiang Gongshang University Hangzhou College of Commerce in 2017. She is now a postgraduate student of the School of Big-data Science, Zhejiang University of Science and Technology. Her research interests include deep learning and machine learning security.



**Bin Wang**, Ph.D., Senior Engineer, he is the Vice President of Hangzhou Hikvision Digital Technology Co., Ltd. His research interests mainly include new computer networks, artificial intelligence security, Internet of Things security and so on. In these areas he has published more than 50 papers in international journals or conferences. He is the member of CCF (China Computer Federation) and CIE (The Chinese Institute of Electronics)



**Zhaoquan Gu** received his bachelor degree in Computer Science from Tsinghua University (2011) and PhD degree in Computer Science from Tsinghua University (2015). He is currently a professor in the Cyberspace Institute of Advanced Technology (CIAT), Guangzhou University, China. His research interests include wireless networks, distributed computing, big data analysis, and artificial intelligence security.



**Xiang Ling** received the B.E. degree from the China University of Petroleum (East China) in 2015. He is currently pursuing the Ph.D. degree with the College of Computer Science and Technology, Zhejiang University. His research mainly focus on the data-driven security, AI security and graph neural network.



**Chunming Wu** received the Ph.D. degree in computer science from Zhejiang University in 1995. He is currently a Professor with the College of Computer Science and Technology, Zhejiang University, where he is also an Associate Director of Institute of Computer System Architecture and Network Security of Zhejiang University. His research fields include software-defined networks, reconfigurable networks, proactive network defense, network virtualization and intelligent networks.